Geophys. J. Int. (2005) **161,** 373–386 doi: 10.1111/j.1365-246X.2005.02600.x

Resolution of regional seismic models: Squeezing the Iceland anomaly

Richard M. Allen[1,*†] and Jeroen Tromp[2]

[1] *University of Wisconsin–Madison, WI, USA*
[2] *California Institute of Technology, Pasadena, CA, USA*

Accepted 2005 February 7. Received 2004 December 5; in original form 2004 February 3

SUMMARY

We present a resolution study of the velocity structure beneath Iceland as constrained by teleseismic traveltime tomography using data from the HOTSPOT seismic network. This temporary PASSCAL network and the tomographic technique that was used to generate the ICEMAN velocity models are typical of regional seismic studies. Therefore, this study also provides a basis for understanding the resolution of other regional seismic experiments. A suite of tests is used to constrain the range of velocity models that satisfy the traveltime observations on Iceland. These include ray-theoretical squeezing experiments, which attempt to force velocity anomalies into specific geometries while still satisfying the data set, and finite-frequency experiments, which use the spectral-element method (SEM) to simulate full waveform propagation through various 3-D velocity models. The use of the SEM allows the verification of the ray-theoretical ICEMAN models without the assumption of ray theory. The tests show that the ICEMAN models represent an end-member of the range of velocity models that satisfy the data set. The 200-km-width Gaussian-shaped upwelling beneath Iceland, imaged in the ICEMAN models, is at the broadest end of the allowed model range; the peak −2 per cent compressional and −4 per cent shear wave perturbations are lower bounds on the amplitude of the velocity model. Such broadening and lowering of velocity anomalies is the product of data coverage, the ray-theory approximation and regularization of the inversion. Comparison of the traveltime delays produced by a 100-km-diameter conduit as measured at short (1 s) and long (∼20 s) periods demonstrate that such a conduit cannot satisfy the observed traveltime delays. Thus the width of the upwelling conduit beneath Iceland must lie in the range of 100 to 200 km. Separate tests on the minimum depth extent of the anomaly show that significant low velocities are required to 350 km depth. Should the true conduit be at the narrower end of the possible range, both compressional and shear wave perturbations greater than 10 per cent would be required to depths of at least 350 km. Mineral physics experiments indicate that such velocity anomalies would in turn require the presence of partial melt or some other fluids to these depths. These bounds on the allowed velocity structure beneath Iceland provide a constraint on geodynamic models for the generation of the Iceland hotspot, whether it is the result of a top-down or bottom-up process.

Key words: Iceland, ray theory, resolution, seismic tomography, spectral-element method.

1 INTRODUCTION

Seismic tomography is a powerful technique able to constrain 3-D crust and mantle structure. However, the produced velocity models include artefacts as a result of both inherent inaccuracies in the applied methods and subjectively chosen filters. The central role these snapshots of Earth structure play in our interpretation of the geodynamic processes that operate makes it vitally important that we understand the uncertainties in these images and the variety of velocity models that can satisfy a constraining data set. In this study, we determine the range of 3-D velocity models that satisfy a regional teleseismic body wave traveltime data set derived from the HOSTPOT network deployed across Iceland (Allen *et al.* 1999). The data set was previously used in a tomographic experiment that employed ray theory to determine the velocity structure in the mantle beneath Iceland to a depth of 400 km (Allen *et al.* 2002a). We build on the Allen *et al.* (2002a) study by testing for the range of velocity

*Now at: University of California Berkeley, CA, USA
†Corresponding author: Dept Earth & Planetary Science, University of California Berkeley, 215 McCone Hall, Berkeley, CA 94720-4760, USA. E-mail: rallen@berkeley.edu

models that satisfy the traveltime data set using both ray-theoretical and finite-frequency techniques, and provide specific bounds on the geometry of velocity structures that may be present beneath Iceland. The resolution tests also provide a guide for interpretation of similar regional tomographic studies. The network geometries of many regional seismic deployments facilitated by the PASSCAL instrument pool are very similar to the HOTSPOT network that provided the data set for this study. Limitations in the resolution and artefacts in tomographic images are therefore also similar.

Estimation of the possible range of velocity structures beneath Iceland is important to the ongoing debate over the causal mechanism for the Iceland hotspot. Iceland was on Morgan's initial list of hotspots hypothesized to be the result of plumes of hot mantle material rising from the core–mantle boundary region (Morgan 1971). Since that time there have been many geophysical and geochemical studies focused on the mantle beneath Iceland. Perhaps the most important geochemical observation that indicates a deep mantle source for the melting anomaly is the high ^{3}He/^{4}He ratios. Breddam *et al.* (2000) identify a plateau of high values in central Iceland where the ratios are ∼20 times atmospheric. However, the association of high ^{3}He/^{4}He ratios with a reservoir distinct from that sampled by N-MORB has been questioned (Anderson 2001), as have the locations of such a reservoir in the deep mantle (e.g. Anderson 1993; Graham *et al.* 1996). Regional tomographic experiments show a low-velocity anomaly near cylindrical in shape, 200 to 300 km in diameter and extending to at least the base of the upper mantle, the maximum depth of resolution (Wolfe *et al.* 1997; Foulger *et al.* 2001; Allen *et al.* 2002a; Hung *et al.* 2004). While these observations are consistent with the presence of a mantle plume, proof of a plume requires continuation of the conduit deep into the lower mantle where regional models have no resolution. Global tomography experiments have produced inconclusive evidence of a deep mantle source for Iceland. While some models suggest a low-velocity conduit extending into the lower mantle (Bijwaard & Spakman 1999; Zhao 2001) and others do not (Ritsema *et al.* 1999; Montelli *et al.* 2004), all have horizontal resolutions of ∼1000 km and a narrow conduit of the scale observed in the upper mantle may therefore not be resolvable (Ritsema & Allen 2003). Measurements of transition zone thickness in the North Atlantic show a thinning near Iceland, which is also consistent with the passage of a high-temperature anomaly from the lower to the upper mantle (Shen *et al.* 2002).

While conclusive evidence for the presence of a deep seated plume beneath Iceland remains elusive, should a plume exist, geodynamic models provide images of what it may look like. Early geodynamic models for Iceland exhibited a trade-off between the radius of the plume tail and the temperature anomaly. (Note that all references to conduit radius in this paper refer to the radius at which the best-fitting Gaussian-shaped anomaly falls to 1/e of the peak value.) While broad cool plumes (peak temperature $<100^\circ$C, radius >300 km) were preferred to satisfy topography, crustal thickness and gravity, narrow hot plumes (peak temperature 170°C, radius 60 km) provided the best fit to the ^{87}Sr/^{86}Sr anomaly, considered to be a signature of plume material (Ribe *et al.* 1995; Ito *et al.* 1996). More recent geodynamic models for Iceland have converged on a narrow conduit, which satisfies all surface observables through the inclusion of dehydration effects on mantle viscosity during melting (Ito *et al.* 1999). The increase in viscosity caused by the immediate removal of fluids on initiation of melting causes most of the upwelling material to divert around the melting region. The most recent geodynamic plume models for Iceland have conduits that are ∼50 km in radius (Albers & Christensen 2001; Ito 2001). In contrast, seismic constraints suggest an anomaly that is at least twice a wide as these geodynamic models: both modelling of diffraction effects of the anomaly (Allen *et al.* 1999) and ray-theoretical traveltime tomography experiments (Foulger *et al.* 2001; Allen *et al.* 2002a) suggest a radius of ∼100 km. A more recent tomography model for Iceland that uses finite-frequency sensitivity kernels suggests a broader ∼150-km-radius anomaly (Hung *et al.* 2004). It can be argued that an ultranarrow 50-km-radius conduit could be present beneath Iceland as a result of the various inherent limitations of seismic imaging techniques. We therefore determine the minimum width of any anomaly beneath Iceland necessary to generate the observed traveltime data set.

While many observations are consistent with the presence of a mantle plume beneath Iceland, none provides conclusive proof for a deep mantle origin. Alternative hypotheses for the Iceland hotspot are driven by top-down processes resulting from the separation of the adjacent continents. They involve small-scale convection driven by the lateral thermal gradient developed across the edge of the continent and passive upwelling and infilling of the mantle beneath the new ocean (e.g. King & Anderson 1998; Korenaga & Jordan 2002). However, it is difficult to assess the applicability of these hypotheses to the Iceland hotspot as there are no geodynamic models specifically tailored to observables in the region that exhibit these small-scale convection processes. Two important constraints on future geodynamic models for Iceland will be the depth and horizontal extent of the upwelling. For this reason, we assess both the minimum depth extent of the low-velocity anomaly beneath Iceland, and the minimum and maximum horizontal diameters of the anomaly.

We conduct ray-theoretical and finite-frequency experiments to explore the true range of mantle velocity models that satisfy the seismic observations on Iceland. We use ray-theoretical synthetic resolution and squeezing experiments to test the minimum depth extent of the low-velocity anomaly and to test if an ultranarrow 50-km-radius conduit can satisfy the observed traveltime delays. We then abandon ray theory and use the spectral-element method (SEM), a numerical technique for the simulation of seismic wave propagation through the entire globe, including a 3-D velocity model, to calculate synthetic waveforms for a variety of velocity models. This allows testing of the velocity models generated by ray theory and provides a basis for understanding the limitations of ray theory for a regional tomographic experiment.

2 THE ICEMAN DATA SET AND MODELS

The teleseismic traveltime data set used in this study is identical to that used to generate the ICEMAN models. Generation of the data set and development of preferred tomographic models that represent minimum norm solutions are described in full by Allen *et al.* (2002a). The data set is the product of the HOTSPOT deployment of PASSCAL instruments across Iceland from 1996 July till 1998 August. Waveforms from the permanent South Iceland Lowlands (SIL) network (Stefansson *et al.* 1993) and the temporary ICEMELT deployment (Bjarnason *et al.* 1996) were also used. Fig. 1 shows a map of the combined station distribution. Relative traveltime data sets were generated by cross-correlation of seismic arrivals. *P* and *PKIKP* arrivals were bandpassed between 0.8–2.0 and 0.03–0.1 Hz prior to cross-correlation, providing two compressional arrival-time data sets. *S* and *SKS* arrivals were only detectable in the lower frequency window, providing just one shear arrival-time data set. This low-frequency data set is a little lower than commonly used as a

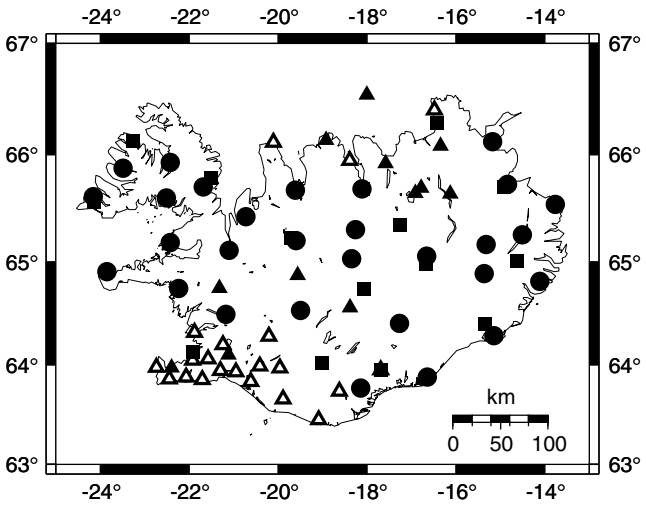

Figure 1. Map of Iceland showing the distribution of seismic stations used in this study. The ICEMAN data sets come from three networks: the HOTSPOT (circles) and ICEMELT (squares) networks, both consisting of broad-band instruments, and the SIL network consisting of broad-band (solid triangles) and short-period (open triangles) instruments.

result of the higher level of microseismic noise in Iceland compared with continental settings. We use the tags ICEMAN-HP and ICEMAN-LP to refer to the high- and low-frequency compressional arrival data sets, which consist of 2695 and 2103 arrivals respectively. We use the tag ICEMAN-S for the low-frequency shear arrival data set, which consists of 1814 arrivals. The three data sets were inverted to produce three velocity models of the mantle beneath Iceland for which we use the same tags: ICEMAN-HP, ICEMAN-LP and ICEMAN-S.

The ICEMAN models were generated using integrated seismic techniques. The teleseismic arrival times were corrected for crustal structure prior to inversion using the crustal model of Allen *et al.* (2002b). Surface waves were used to provide additional constraints on the velocity structure in the upper ∼200 km of the mantle. Inversion of the body wave data sets alone shows a low-velocity anomaly extending from the maximum depth of resolution up to ∼200 km where it apparently stops. The surface wave constraints show the presence of a horizontal low-velocity anomaly that extends beneath all of Iceland. Such an anomaly beneath an entire seismic network cannot be detected using a relative arrival-time data set, which is why it is absent from the body-wave-only tomographic results. Combining the body and surface wave constraints produces a velocity model in which the deeper, vertical low-velocity anomaly connects to a horizontal low-velocity anomaly extending beneath all of Iceland (see fig. 6 of Allen *et al.* 2002a). Allen *et al.* (2002a) interpret the ICEMAN models as a buoyant upwelling originating below the maximum depth of resolution (∼400 km) and feeding mantle material up to the melting zone beneath Iceland. This material then spreads out beneath the lithosphere as it flows horizontally away from the upwelling region. All hypothesized models for the Iceland hotspot must generate buoyant upwelling to support the large volume of volcanism on Iceland and thus result in lateral spreading of the same material beneath the Icelandic lithosphere. It is the geometry of the upwelling anomaly that may vary between mechanisms. In this study, we therefore focus on the geometry of the upwelling conduit of the Iceland low-velocity anomaly (structure below ∼200 km), which is constrained by the teleseismic body wave arrival time data sets alone (with applied crustal corrections).

3 RAY-THEORETICAL RESOLUTION TESTS

We conduct two types of resolution experiments using the ray-theoretical approximation. First, synthetic resolution tests are used to determine whether our data set can resolve specific velocity structures. Secondly, squeezing tests are used to determine the locations of velocity anomalies required by the data.

In synthetic resolution tests a synthetic velocity model is generated and used to calculate a data set. The data set is then inverted to determine if the original velocity structure can be recovered. These tests can only be used to determine whether a specified synthetic structure could be resolved by the data set should it exist in the Earth. They cannot be used to prove that the velocity structure determined from an observed data set is the true structure of the Earth. To illustrate this point, consider a velocity model consisting of six cells with a source on one side and receiver on the other, as shown in Fig. 2(a). If there is a negative velocity perturbation in one of the sampled cells, say −4 per cent, then the arrival at the receiver will be late. If this single traveltime observation represents the data set used in an inversion for the velocity anomalies in all six cells, then the minimum norm solution would consist of a −2 per cent anomaly in the two cells sampled by the ray as shown in Fig. 2(b). As a result of the absence of crossing rays, the low-velocity anomaly is smeared along the ray path. Having completed the inversion, we want to test the resolution of our data set. If we use a synthetic velocity model similar to the inversion result, trace the ray through it to generate a synthetic data set (Fig. 2c) and invert, we will obtain a velocity model that looks like Fig. 2(d), the same as the initial synthetic velocity model. Clearly, this does not demonstrate that the true velocity model looks like the synthetic one: it simply demonstrates that given

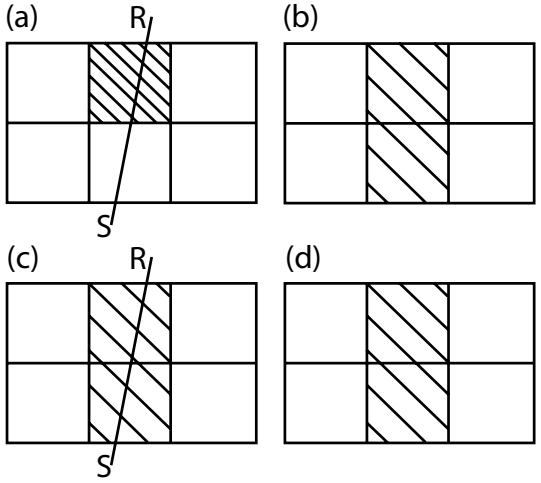

Figure 2. Cartoon to illustrate the limitations of synthetic resolution tests. The model domain consisting of six cells one of which has a −4 per cent velocity anomaly is shown in (a). The (limited) ray-path coverage is indicated by the line SR; the data set consists of one traveltime measurement. The minimum norm solution resulting from inversion of the available traveltime data set is shown in (b): the velocity anomaly is smeared along the ray as a result of the ray coverage resulting in a −2 per cent anomaly in two cells. In an effort to demonstrate that (b) represents the true velocity structure (a), a synthetic velocity model (c) is generated for use in a synthetic resolution test. The synthetic velocity model (c) has been chosen to look like the (b). The synthetic data set is calculated using the same ray path through the synthetic velocity model. Inversion of the synthetic data set produces the solution shown in (d). Although the synthetic velocity model (c) is recovered, this success does not demonstrate that (b) is the true velocity structure.

the available ray coverage it is possible to recover a structure that looks like our inversion result. If, however, we conducted a resolution test where the initial synthetic model looks like Fig. 2(a), we would recover a velocity model like Fig. 2(b), demonstrating that our data set is unable to resolve a structure like Fig. 2(a).

Squeezing experiments are used to test if a hypothetical velocity structure is consistent with a data set. In some ways, it is a more rigorous test of a hypothetical velocity structure than a synthetic resolution test. Synthetic resolution tests are intended to assess if the data set is able to resolve the hypothetical structure, whereas squeezing experiments are used to determine whether it is possible to force, or squeeze, the velocity model, which still satisfies the data set, into the hypothetical geometry. For example, Saltzer & Humphreys (1997) use a teleseismic traveltime data set recorded on instruments across the Snake River Plain (SRP) and seismic tomography to constrain the 2-D velocity structure beneath the array. Their minimum norm solution suggests a low-velocity anomaly 125 km wide and extending to ∼325 km depth. In their subsequent squeezing experiments, they are successful in forcing the velocity structure into the upper 200 km while still satisfying their traveltime data set. It is possible that the apparent continuation of the low-velocity anomaly to ∼325 km depth in their minimum norm solution is the result of either an artefact, such as smearing along near-vertical rays, or it is real, i.e. there are low velocities to ∼325 km in the Earth beneath the SRP. Either way, the data set is unable to resolve if low velocities continue to ∼325 km depth: it only requires low velocities to 200 km depth. Squeezing tests are useful not only for ray-theoretical but also for finite-frequency inversions. The banana-shaped sensitivity kernels (e.g. Dahlen *et al.* 2000; Hung *et al.* 2000; Zhao *et al.* 2000) used in finite-frequency inversions have the effect of smearing any velocity anomaly throughout the banana-shaped kernel in a similar fashion to how ray-theoretical inversions smear velocity anomalies along the rays. Finite-frequency kernels suffer the same limitations in depth resolution for regional teleseismic studies as ray theory. Squeezing tests can therefore be used to determine if a velocity anomaly could be isolated within just one part of the kernel volume while still satisfying the data (see Section 5).

We present the results of a series of squeezing experiments designed to test both the depth and horizontal extent of the velocity anomaly beneath Iceland. Squeezing is implemented through the use of a two-stage inversion. In the first stage, velocity anomalies are permitted within a specific region of the model, such as a depth range. Non-zero model parameters are prohibited from other regions through an effectively infinite damping parameter. The linear system solved is therefore

$$\begin{bmatrix} \mathrm{A} \\ \Gamma \end{bmatrix} \mathbf{x_1} = \mathbf{d}, \tag{1}$$

where $\mathbf{x}_1$ is the slowness model vector, $\mathbf{d}$ is the arrival time data vector, A is a matrix expressing the sensitivity of each data value to the model and Γ is the diagonal matrix of damping parameters. Rather than using a constant damping factor for all model parameters, damping factors corresponding to model parameters where velocity anomalies are not to be permitted are set to a very large value. After the first stage inversion, the residual data vector, i.e. traveltime delays that cannot be satisfied with velocity anomalies within the permitted region, is calculated:

$$\mathbf{r_1} = \mathbf{d} - \mathrm{A}\mathbf{x_1}. \tag{2}$$

In the second-stage inversion, velocity anomalies are allowed throughout the model in order to satisfy $\mathbf{r}_1$. We solve the system

$$\mathrm{A}\mathbf{x}_2 = \mathbf{r_1}. \tag{3}$$

The final model solution $\mathbf{x}$ is simply the sum of $\mathbf{x}_1$ and $\mathbf{x}_2$, and the final misfit to the data is

$$\mathbf{r} = \mathbf{r_1} - \mathrm{A}\mathbf{x_2} = \mathbf{d} - \mathrm{A}\mathbf{x_1} - \mathrm{A}\mathbf{x_2} = \mathbf{d} - \mathrm{A}\mathbf{x}. \tag{4}$$

The velocity models resulting from these tests satisfy the constraining data set equally well, i.e. the rms of the misfit vector $\mathbf{r}$ is approximately the same after each test. The difference is that the solutions are no longer minimum norm solutions.

3.1 Depth extent of the low-velocity anomaly

The maximum depth of resolution in regional tomographic studies is approximately equal to the aperture of the seismic network. The HOTSPOT deployment across Iceland was limited by the aerial extent of Iceland, which is approximately 300 km by 500 km (Fig. 1). We therefore expect resolution to ∼400 km depth. Fig. 3 shows the results of both synthetic resolution tests and squeezing experiments designed to determine the minimum depth extent required by this data set of the low-velocity anomaly beneath Iceland.

The four synthetic velocity models consist of vertical cylinders with a 75-km-radius Gaussian-shaped low-velocity anomaly. Each has a 100 km depth extent and is placed at various depths (Fig. 3, left column). The recovered velocity anomalies (Fig. 3, middle column) are lower in amplitude as a result of the damping imposed in the inversion. Fig. 3 shows the results of tests using the shear wave arrival-time (ICEMAN-S) data set, though the same tests using the ICEMAN-LP and ICEMAN-HP data sets exhibit similar resolution. The geometry of the input velocity anomalies is recovered very well: the horizontal width of the input and recovered anomalies are the same. Given that teleseismic ray paths are closer to vertical than horizontal at these depth ranges, vertical smearing is more of a concern than horizontal smearing. Fig. 3 shows that vertical smearing is minimal for this data set. While the input peak-velocity anomaly $V_{S\max} = -5$ per cent in each case, the recovered peak anomalies are approximately −2.5 per cent above 300 km depth, −1.5 per cent at 300–400 km and −1 per cent at 400–500 km depth. This demonstrates the relatively good resolution to 300 km and reasonable resolution from 300 to 400 km. These tests use relatively small velocity anomalies, approximately equal to 100-km-diameter spheres. The minimum norm ICEMAN solutions (Fig. 3 top right shows a slice through ICEMAN-S) resolve velocity anomalies with lengthscales greater than twice these test cases. The fraction of the amplitude of the input velocity anomaly recovered increases with the volume of the anomaly. When a 100-km-radius vertical cylinder is used as the input, 70 to 80 per cent of the peak velocity anomaly is recovered (Allen *et al.* 2002a).

Squeezing experiments are used to test the minimum depth extent required by the data set. In each test, velocity anomalies are permitted within a specified 100 km depth range in the first stage inversion and throughout the model region during the second stage. The results of squeezing ICEMAN-S into the same depth ranges used for the synthetic resolution tests are shown in Fig. 3 along with the minimum norm solution for comparison (right column). In each case, larger-amplitude velocity anomalies are obtained within the target depth range. Significant low-velocity anomalies are also required to at least 350 km depth in every case. The minimum depth extent of the Iceland low-velocity anomaly, as required by this data set, is therefore 350 km. Note that the apparent absence of low velocities above ∼200 km depth is the result of the presence of a low-velocity anomaly extending beneath all of Iceland. Such a low-velocity anomaly cannot be resolved using relative arrival-time tomography (see discussion in Section 2).

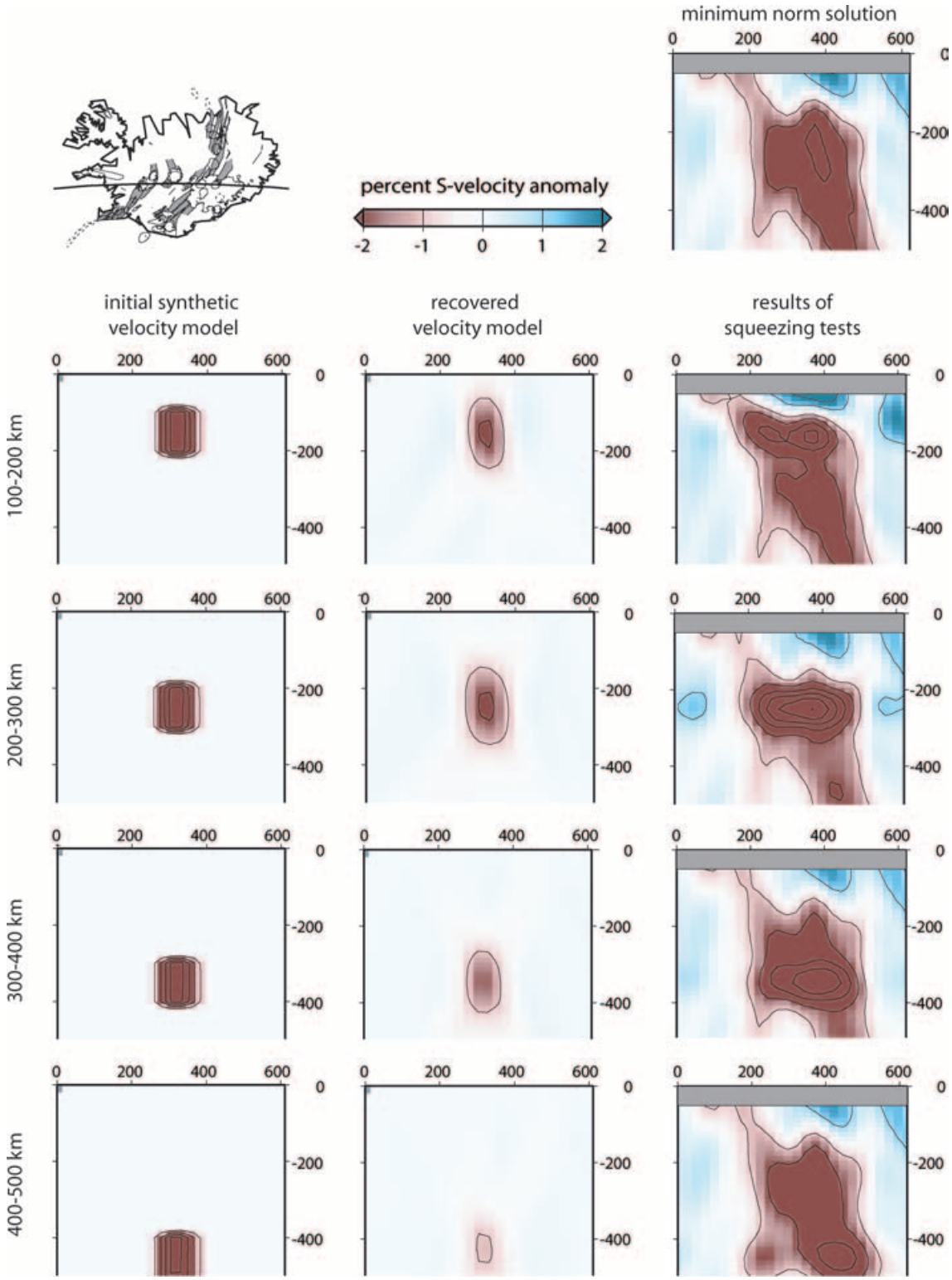

Figure 3. Results of resolution experiments to test the depth extent of the low-velocity anomaly beneath Iceland required by the ICEMAN-S data set. All plots show east–west vertical cross-sections in the location indicated on the map insert. Synthetic velocity models with low-velocity blobs at various depths (left column) were used as the input for synthetic resolution tests. The recovered velocity models are shown adjacent (middle column), and indicate good resolution to 300 km depth and acceptable resolution to 400 km depth. The results of squeezing experiments (right column), in which velocity anomalies were squeezed into the same depth ranges as the synthetic tests, indicate that the data set requires low velocities to a minimum of ∼350 km depth. The same slice through the minimum norm ICEMAN-S model is shown top-right.

3.2 Diameter of the upwelling conduit

The synthetic resolution tests shown in Fig. 3 demonstrate that velocity anomalies with horizontal lengthscales much smaller than the velocity anomaly beneath Iceland can be resolved. To test how narrow the upwelling conduit beneath Iceland could be, we conduct squeezing experiments in which velocity anomalies are only permitted within a vertical cylinder 100 km wide and centred beneath central Iceland. Fig. 4 shows the minimum norm solutions (left column) and the results of the squeezing experiments (right column) for models ICEMAN-S and ICEMAN-HP. This ray-theoretical test of the low-frequency data set ICEMAN-S prohibits a narrow conduit of this kind, as the data still require significant low velocities over a broader region. The results of the test on the high-frequency, ICEMAN-HP, data set are very different; the low-velocity anomaly is successfully forced into a 100-km-wide conduit. This would imply that the ICEMAN-HP data set can be satisfied by a 100-km-wide conduit, while the ICEMAN-S data set requires a much broader conduit approximately 200 km wide. The same test was performed on the ICEMAN-LP data set; the result was similar to the ICEMAN-S data set in that low velocities are required over a region broader than the 100 km cylinder.

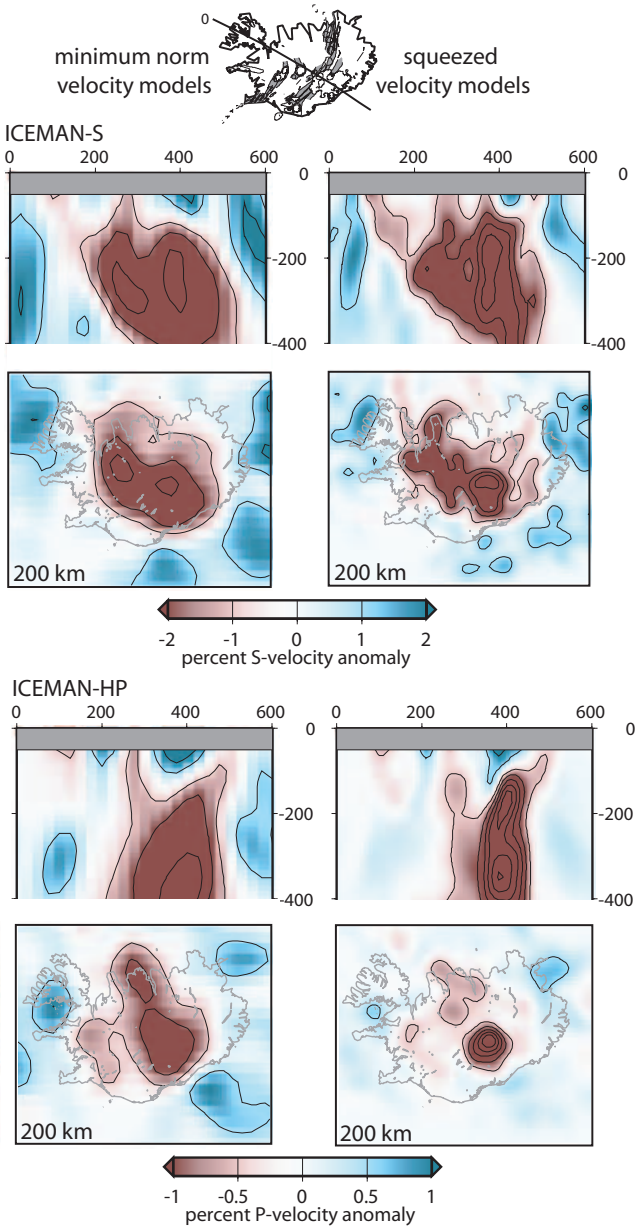

Figure 4. Results of squeezing experiments designed to test the minimum horizontal width of the low-velocity conduit permitted by the data. The same slices through the ICEMAN-S and ICEMAN-HP minimum norm solutions (left column) and the results of squeezing the velocity models into vertical cylinders 100 km wide (right column) are shown. While significant low-velocity anomalies are required over a region broader than 100 km for the low-frequency ICEMAN-S data set, this is not the case for the high-frequency ICEMAN-HP data set.

The two possible explanations for these observations are:

(i) the geometry of the compressional- and shear-velocity anomalies are different; and

(ii) the different frequency content of the two data sets results in different images of the same velocity anomaly.

Given the similarity of the low-frequency compressional- and shear-velocity models, we reject the first possibility and focus on the second. The ray-theoretical approximation used in these squeezing experiments associates the measured traveltime anomaly with velocity anomalies along an infinitely narrow ray. The traveltime anomaly is in fact sensitive to velocity anomalies in a finite volume around the ray approximately equal to the Fresnel zone (e.g. Hung *et al.* 2001). The width of the Fresnel zone, perpendicular to the ray, is wavelength-dependent. Ray theory is an infinite-frequency approximation; it is accurate for infinite-frequency arrivals, which have zero wavelength and therefore zero-width Fresnel zones. There is an order of magnitude difference in the wavelengths of the ICEMAN-HP and ICEMAN-S data sets, which have wavelengths of the order 10 and 100 km, respectively. Given a narrow conduit beneath Iceland and a ray path that misses the anomaly by, say, 50 km, the high-frequency *P* arrival would not be sensitive to the anomaly while the longer wavelength *S* arrival would be. We therefore expect the width of the ICEMAN-S anomaly to be greater than the ICEMAN-HP anomaly and the ICEMAN-HP anomaly could be squeezed into a much narrower conduit than the ICEMAN-S anomaly, which is what we observe. We therefore propose the hypothesis that the anomaly beneath Iceland is much narrower than imaged in the ICEMAN models. Given that the artificial broadening is the result of finite-frequency effects ignored by ray theory, testing of this hypothesis requires the abandonment of ray theory.

4 ABANDONING RAY THEORY

The spectral-element method (SEM) provides a method for the simulation of global seismic wave propagation that accurately incorporates 3-D velocity heterogeneity without any limit on the level of heterogeneity or the applicable frequency range. It is a forward calculation that provides synthetic waveforms generated by a finite source at some specified location and accurately propagates the waveform through the specified global 3-D velocity structure. The method is described in detail by Komatitsch & Tromp (2002a,b); a useful overview is provided by Komatitsch *et al.* (2002).

The waveform propagation experiments presented here use an implementation of the SEM on a cluster of personal computers consisting of 150 processors and 75 GB of memory. While the SEM imposes no intrinsic upper limit on the frequency content of the synthetics, memory availability does. Our simulations provide accurate synthetics at periods greater than 12 s allowing calculation of synthetics at similar frequencies to the ICEMAN-S and

ICEMAN-LP data sets. We are unable to generate SEM-synthetic data sets at ∼1 s relevant for the ICEMAN-HP data set. We can assess the significance of non-ray-theoretical (i.e. finite frequency) effects given the propagation of a seismic wave with wavelength λ through a Gaussian-shaped velocity anomaly with half-width L, using the ratio L/λ. When $L/\lambda \leq 1$, finite-frequency effects become significant (Nolet & Dahlen 2000). For a period of 20 s and an L of 50 km (similar to the narrow conduit used in the squeezing experiments of Section 3.2), L/λ is 0.3 and 0.5 for compressional and shear waves respectively, indicating significant finite-frequency effects; at 1 s, L/λ is 5.7 for compressional waves. This suggests that ray theory is a good approximation for the ICEMAN-HP data set but not for the ICEMAN-LP or ICEMAN-S data sets. We can therefore use the SEM to test velocity models as sampled by 20-s data and ray theory to test the 1 s sampling of the same models.

4.1 ICEMAN verification

We first test the ability of the ICEMAN models to recreate the traveltime data set from which they were generated using the SEM. The ICEMAN-S and ICEMAN-LP relative velocity models were superimposed on the 1-D Earth velocity model Preliminary Reference Earth Model PREM (Dziewonski & Anderson 1981). As the ICEMAN velocity models were generated from teleseismic traveltime data sets, which were corrected for crustal traveltimes using the ICECRTb crustal model (Allen *et al.* 2002b), we also added ICECRTb to the SEM velocity grid. A typical earthquake was selected to compare SEM-synthetic waveforms with those recorded by the HOTSPOT network. The 1997 July 9 event, a magnitude 7.0 earthquake off the coast of Venezuela (latitude 10.428°N, longitude 63.486°W, depth 10 km), is at an epicentral distance of 62° from the centre of the network, which is approximately the average epicentral distance of events providing *P* and *S* arrivals in the ICEMAN data sets. Synthetic waveforms were calculated at the same locations as where the HOTSPOT stations were deployed. Fig. 5 shows comparisons of the *P* and *S* arrivals on the observed and synthetic waveforms. The observed data are the raw waveforms; the vertical axis is in counts. To obtain equivalent synthetics, the SEM synthetics were convolved with the instrument response of each HOTSPOT station. The *P* and *S* waveforms are very similar: the agreement in the amplitude of the synthetic and observed arrivals is good. The waveform complexity of the recorded data after the first swing of the *P*- and *S*-wave arrival (>30 s after the arrivals) is not observed in the synthetics. This complexity is not the result of the source time function (on account of its lateness) but is observed on waveforms recorded across Iceland and the adjacent Atlantic margins. It is therefore most likely the result of near-source structure, which we do not attempt to model.

To test the accuracy of the ICEMAN models, we use the same cross-correlation technique used on the data to measure the relative arrival times of the *P* and *S* phases in SEM synthetics (Allen *et al.* 2002a). Only the first swing of the arrival is included in the cross-correlation window preventing contamination of the relative traveltimes by the later waveform complexity. Fig. 6 shows the relative delay times, having corrected for epicentral distance. The observed delays across Iceland are plotted against the SEM-synthetic delays for the *P* and *S* arrivals. The low-velocity anomaly beneath Iceland causes a total delay across the network of ∼1 and ∼3 s for the *P* and *S* arrivals, respectively, for this earthquake. It is these gross delays that require a low-velocity anomaly beneath Iceland. If the ICEMAN models were a perfect representation of the Earth, all points in Fig. 6 would fall along the line shown. To measure the error in the SEM-synthetic delay times, we calculate the SEM-synthetic residuals: the difference between the observed delays and the SEM-synthetic delays. The rms values of these residuals are shown in Table 1 along with the observed data rms. The ICEMAN-LP velocity model reduces the rms residuals by 56 per cent from 0.34 to 0.15 s. This is very similar to the 60 per cent rms reduction (0.34 to 0.13 s) obtained using ray theory to calculate the synthetic traveltimes through ICEMAN-LP. The similarity of these results demonstrates:

(i) the validity of the ICEMAN-LP model in that it still satisfies the traveltime data set when we use full 3-D waveform propagation (i.e. the SEM) to calculate traveltimes rather than the ray-theoretical approximation; and

(ii) ray theory does provide a valid solution in this regime where we should be concerned about the validity of ray theory.

Comparison of the ray-theoretical and SEM-synthetic residual rms values for ICEMAN-S is not as favourable (Table 1). The ray-theoretical residual rms is 0.26 s, reduced from 1.04 s, while the SEM residual rms is higher at 0.52 s. Despite this difference, we suggest that the SEM-synthetic residual rms is still satisfactory, as the ray-theoretical rms residual for the entire ICEMAN-S data set is 0.50 s, similar to the SEM-synthetic value for the Venezuela event. The ray-theoretical rms value of 0.26 s for arrivals from the Venezuela earthquake is unusually low. Finally, we compare the ray-theoretical and SEM-synthetic residuals for any correlation in Fig. 7. The lack of correlation suggests that these residuals represent components of the velocity structure of the Earth that are beyond both of our modelling techniques. Correlation of these residuals could indicate an inappropriate regularization of the original inversion.

4.2 Diameter of the upwelling conduit

In this section we aim to test the effects of the ray-theoretical approximation on the apparent diameter and amplitude of the low-velocity conduit beneath Iceland. Vertical low-velocity cylinders with Gaussian-shaped velocity anomalies extending to 600 km depth are used to calculate both ray-theoretical and SEM-synthetic traveltime delays. The ICEMAN models are best approximated by a Gaussian-shaped cylinder with a radius of 100 km and peak velocity anomalies $V_{P\max} = -2$ per cent and $V_{S\max} = -4$ per cent for compressional and shear waves, respectively. The ray-theoretical delay times are shown in Figs 8(a) and (g). The delay maps show a shadow behind the low-velocity anomaly with a width (in the east–west direction) equal to the width of the velocity anomaly. The width of the SEM-synthetic delay shadow for the same velocity models is greater (Figs 8b and h) as seismic arrivals with ray paths that apparently miss the velocity anomaly are delayed as a result of the finite width of their true sensitivity perpendicular to the ray.

To compare the ray-theoretical and SEM-synthetic delay maps, we calculate the percentage of the ray-theoretical delay recovered in the SEM delay map (Figs 8c and i). These maps clearly indicate the broader SEM-synthetic delay footprint compared to ray-theoretical footprint (shown as white regions). The effect of wave front healing (Wielandt 1987) is also evident because the SEM-synthetic delays directly behind the centre of the velocity anomaly are relatively small, reaching only ∼80 per cent of the ray-theoretical value for *S*-wave arrivals (Fig. 8c) and ∼50 per cent for *P*-wave arrivals (Fig. 8i). These differences between ray-theoretical and SEM-synthetic delays indicate that the use of ray theory in any technique to constrain a velocity anomaly will result in a broader, lower amplitude anomaly than in the Earth. This is the result of the fact that

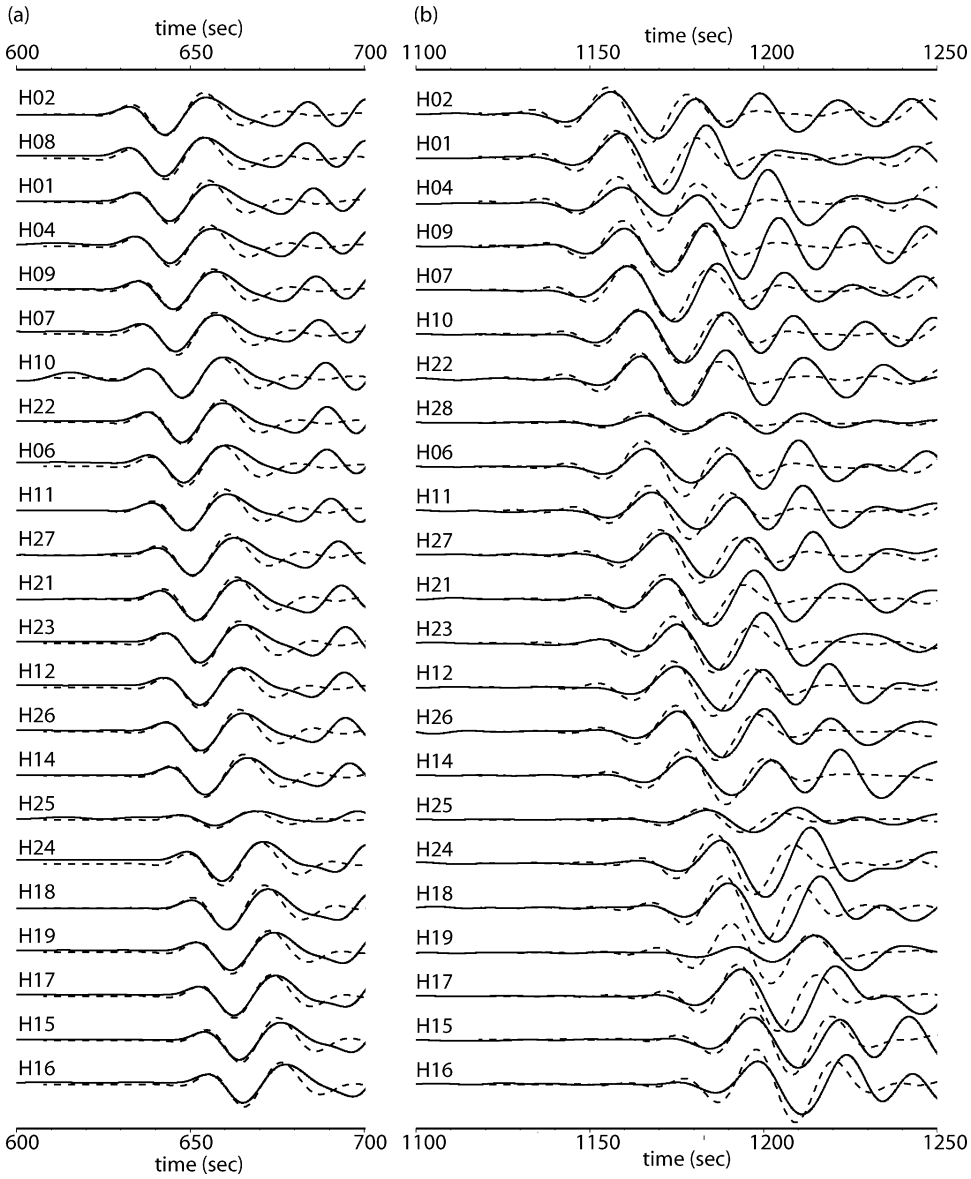

Figure 5. Comparison of *P* and *S* arrivals on the observed (solid) and SEM-synthetic (dashed) vertical component waveforms recorded and calculated for a magnitude 7.0 earthquake off the coast of Venezuela. (a) *P* arrivals on the vertical component. There is good agreement in both the time and amplitude of the arrivals (vertical axes are all on the same scale). (b) *S* arrivals on the tangential component. The agreement in both the time and amplitude of the arrivals is not as good as the *P* arrivals. The additional complexity of the observed data after the *S*-wave arrival (>30 s after the arrival) is most likely the result of near-source structure, which we do not attempt to model.

a traveltime observation is sensitive to a broad region of the subsurface. A traveltime delay map will therefore show delays over a larger area than the causal velocity anomaly. When ray theory is used to construct a velocity model, the resulting velocity anomaly will have similarly expanded spatial extent. This effect is in addition to the broadening and reduction in amplitude of a velocity anomaly as a result of smoothing and damping imposed in an inversion.

Given that ray theory predicts broader, lower amplitude velocity anomalies for a given set of traveltime delays, we consider a narrower, larger amplitude velocity anomaly, and calculate the ray-theoretical and SEM-synthetic delay maps. The squeezing experiments described in Section 3.2 show that the ICEMAN-HP data set can be satisfied by a low-velocity conduit 100 km wide with $V_{P\max} = -3$ per cent. We therefore calculate synthetic delay maps for a 50-km-radius Gaussian-shaped cylinder with $V_{P\max} = -3$ per cent and $V_{S\max} = -6$ per cent. A comparison of the ray-theoretical delay maps for the 50-km-radius anomalies (Figs 8d and j) with the 100-km-radius anomalies (Figs 8a and g) shows that it is half the width with slightly smaller maximum delay times. The SEM-synthetic delay footprints (Figs 8e and k) are much broader than their ray-theoretical equivalents and only marginally narrower than the SEM-synthetic delay footprints for the 100-km-radius velocity anomalies. The wave front healing effect is also more significant for the narrower velocity anomaly than the broader one: ∼60 per cent of the ray-theoretical delay is recovered for *S* arrivals and only ∼40 per cent for *P* arrivals.

To test if the use of a ray-theoretical inversion results in projection of the traveltime delays from a 50-km-radius ($V_{P\max} = -3$ per cent, $V_{S\max} = -6$ per cent) anomaly into a 100-km-radius ($V_{P\max} = -2$ per cent, $V_{S\max} = -4$ per cent) anomaly, we compare

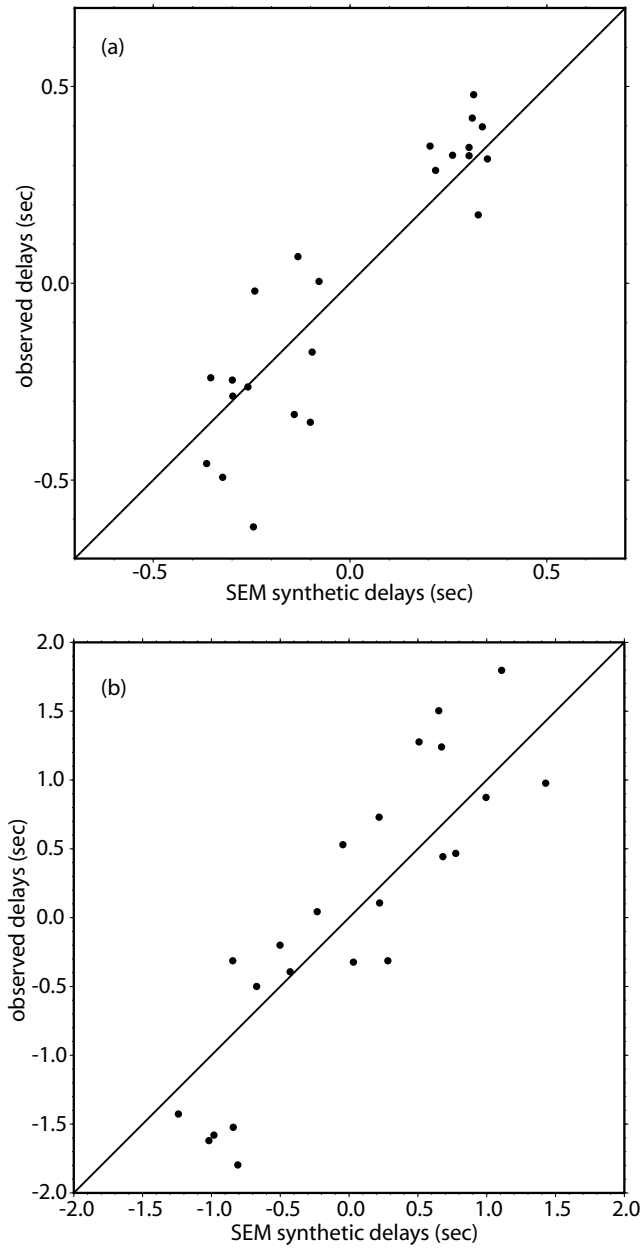

Figure 6. Comparison of observed and SEM-synthetic delay times for the earthquake in Venezuela (1997 July 9; *M* 7.0; 10.428°N, 63.486°W; depth 10 km). (a) *P*-arrival delays, (b) *S*-arrival delays. All delays were calculated by cross-correlation.

the ray-theoretical delays from the 100-km anomalies to the SEM-synthetic delays from the 50-km anomalies. The percentage of the ray-theoretical delays recovered in the SEM-synthetic delay maps are shown in Fig. 8(m) for *S* arrivals and in Fig. 8(n) for *P* arrivals. The east–west widths of the delay footprints are nearly identical for the *P* arrival comparison and very similar for *S* arrivals. This similarity would suggest that it is possible for an apparent 100-km-radius anomaly in the upper few hundred kilometres of the mantle resulting from a ray-theoretical inversion to be the product of a 50-km-radius anomaly in the Earth. However, the true amplitude of the velocity anomaly would also be significantly larger. Given that only ∼60 per cent of the ray-theoretical delay time is recovered for *S* arrivals and ∼30 per cent for *P* arrivals, the velocity anomalies would need to be of the order of 170 per cent of the apparent shear velocity and 330 per cent of the apparent compressional velocity.

Based on these tests, we could argue that the apparent 100-km-radius anomalies beneath Iceland could in fact be much narrower, i.e. 50 km in radius. However, this would require very large peak velocity anomalies of the order of $V_{S\max} = -10$ per cent and $V_{P\max} = -20$ per cent. If the only traveltime data sets available were at low frequencies (greater than 16 s), where the finite-frequency effects investigated here are significant, we would not be able to rule out ultranarrow, ultralow-velocity anomalies. However, in the case of Iceland, the availability of the higher frequency (∼1 Hz) compressional-arrival data set provides additional constraints. The ray-theoretical approximation is satisfactory for the ICEMAN-HP data set, so any velocity anomaly proposed based upon these SEM tests must also generate ray-theoretical traveltime delays that satisfy the observed ICEMAN-HP data set. The squeezing test outlined in Section 3.2 indicates that a 50-km-radius conduit can satisfy the data set but the peak velocity anomaly in this case is around −3 per cent. Increasing the velocity anomaly to −20 per cent would no longer satisfy the data set, therefore a 50-km-radius anomaly cannot satisfy the ICEMAN data sets. While the anomaly beneath Iceland cannot be as narrow as 50 km, the comparisons of the ray-theoretical and SEM-synthetic delay maps in Fig. 8 suggest that the anomaly is narrower than it appears in the ICEMAN models.

4.3 Early arrivals from low-velocity anomalies

The SEM-synthetic delay maps (Figs 8b, e, h and k) show areas with a negative delay, i.e. early arrivals, most visible to the east and west of the velocity anomaly but also wrapping around and in front of the low-velocity anomaly. This observation is perhaps surprising given that the velocity models used to calculate the synthetics include only low-velocity anomalies. The observation is, however, predicted by banana-doughnut traveltime sensitivity kernels (Dahlen *et al.* 2000;

Table 1. Comparison of observed and synthetic rms delay residuals. Residuals are obtained by forward calculation of synthetic traveltimes through the ICEMAN models, which are then subtracted from the observed delays. Both ray theory and the SEM are used for the forward calculation for comparison. The rms values are shown for just the Venezuela earthquake (1997 July 9; *M* 7.0; 10.428°N, 63.486°W; depth 10 km) and the entire ICEMAN data sets. All rms values are in seconds.

	Venezuela event		Entire ICEMAN data sets	
	ICEMAN-LP	ICEMAN-S	ICEMAN-LP	ICEMAN-S
Observed data delays	0.34	1.04	0.50	1.62
Ray-theoretical residuals	0.13	0.26	0.24	0.50
SEM-synthetic residuals	0.15	0.52		

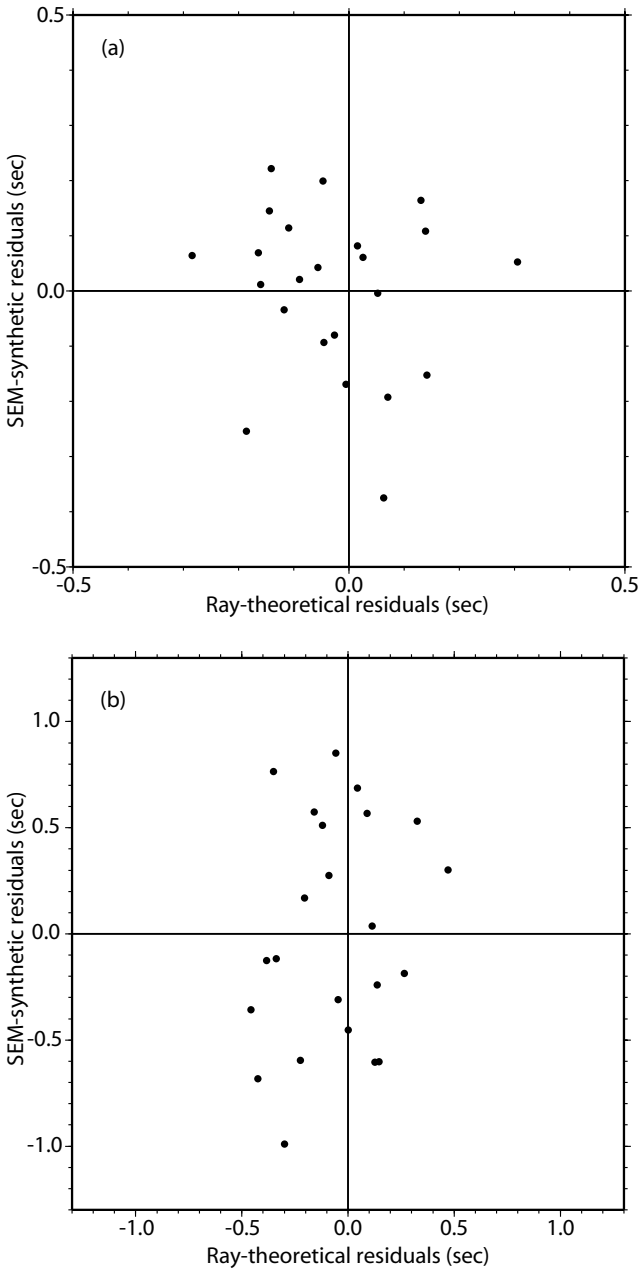

Figure 7. Comparison of SEM-synthetic residuals and ray-theoretical residuals for the earthquake in Venezuela (1997 July 9; M 7.0; 10.428°N, 63.486°W; depth 10 km). (a) P-arrival residuals, (b) S-arrival residuals. The residuals represent the component of each delay time that is not satisfied by the velocity model as calculated using the SEM and ray theory.

Hung *et al.* 2000, 2001). The banana-shaped kernels have alternating positive and negative layers: outside the zero sensitivity core is a layer of negative sensitivity (a negative velocity perturbation results in a positive delay time) corresponding to the first Fresnel zone. Outside the negative sensitivity layer is a positive sensitivity layer (a negative velocity perturbation results in a negative delay, i.e. an early arrival) corresponding to the second Fresnel zone. While the ray-paths associated with these negative delays on the SEM delay maps in Fig. 8 do not traverse the low-velocity anomaly, the first positive sensitivity layer of the banana-doughnut kernel touches the velocity anomaly, resulting in an early arrival.

5 DISCUSSION

Regional seismic deployments are widely used to constrain mantle structures on scales of tens to hundreds of kilometres. These constraints provide the link between larger scale mantle processes, as imaged by global tomography, and smaller-scale processes observed in the crust. The resolution experiments presented above indicate the extent to which regional velocity models can be molded while still satisfying the traveltime data set from which they are generated. This provides a warning against overinterpretation of single preferred velocity models. Such models are usually minimum norm solutions, a choice that biases our perception of mantle structure towards one of broad, low-amplitude velocity anomalies. This bias is the result of:

(i) limited data coverage, which results in smearing of velocity anomalies along ray paths;

(ii) the use of ray theory, which will always broaden velocity anomalies as a result of the finite width of the Fresnel zone; and

(iii) the regularization imposed on the inversion, which usually includes both further smoothing and damping.

Resolution tests, the aim of which is to validate the model, have their limitations as they often use the same approximations as the initial tomographic inversion. The spatial variation in the scale of anomalies that can be resolved given the available data coverage can be assessed using a suite of spike or blob-like synthetic velocity models. The presence of hypothetical structures can also be discounted when the hypothetical structure is resolved in a resolution test but does not appear in the velocity model. However, the successful recovery of a velocity model does not demonstrate its uniqueness. Squeezing experiments allow for a better assessment of the range of velocity models that satisfy a particular data set. As with synthetic resolution tests, squeezing experiments allow hypothetical velocity structures to be discounted. They also begin to allow testing of the validity of a velocity model in that they provide an assessment of the sensitivity of the data set to alternative geometries. Both synthetic resolution tests and squeezing experiments still use ray theory and are therefore not sensitive to the limitations of the approximation.

Investigating the effect of using ray theory on imaged mantle velocity structure is possible using full 3-D waveform propagation techniques. The SEM calculations above illustrate the significance of finite-frequency effects in regional tomographic experiments. For a traveltime measurement at a given frequency, the significance of finite-frequency effects increases as the lengthscale of the velocity anomaly decreases (Nolet & Dahlen 2000). Our calculations of traveltime delay maps using ∼20 s arrivals show that finite-frequency effects are significant for structures in the upper mantle on the scale of tens of kilometres but become less important for anomalies greater than a few hundred kilometres in width. The upper mantle is the target region of most regional tomographic experiments and ∼20 s represents a typical frequency for the measurements of teleseismic arrivals. These finite-frequency effects can result in anomalies up to ∼100 km wide appearing up to twice their true width. The amplitude of the velocity anomaly is also significantly reduced, in some cases by more than 50 per cent. While ray theory provides a good approximation for high-frequency (∼1 Hz) arrivals, it is difficult to measure any teleseismic shear arrivals at these high frequencies. It is also difficult to measure such high-frequency compressional arrivals in ocean bottom deployments. Therefore, we cannot avoid the need to account for finite-frequency effects in our interpretation of regional tomographic velocity models.

Despite the limitations of ray theory, SEM calculations of the traveltime delays generated by the ICEMAN models produce

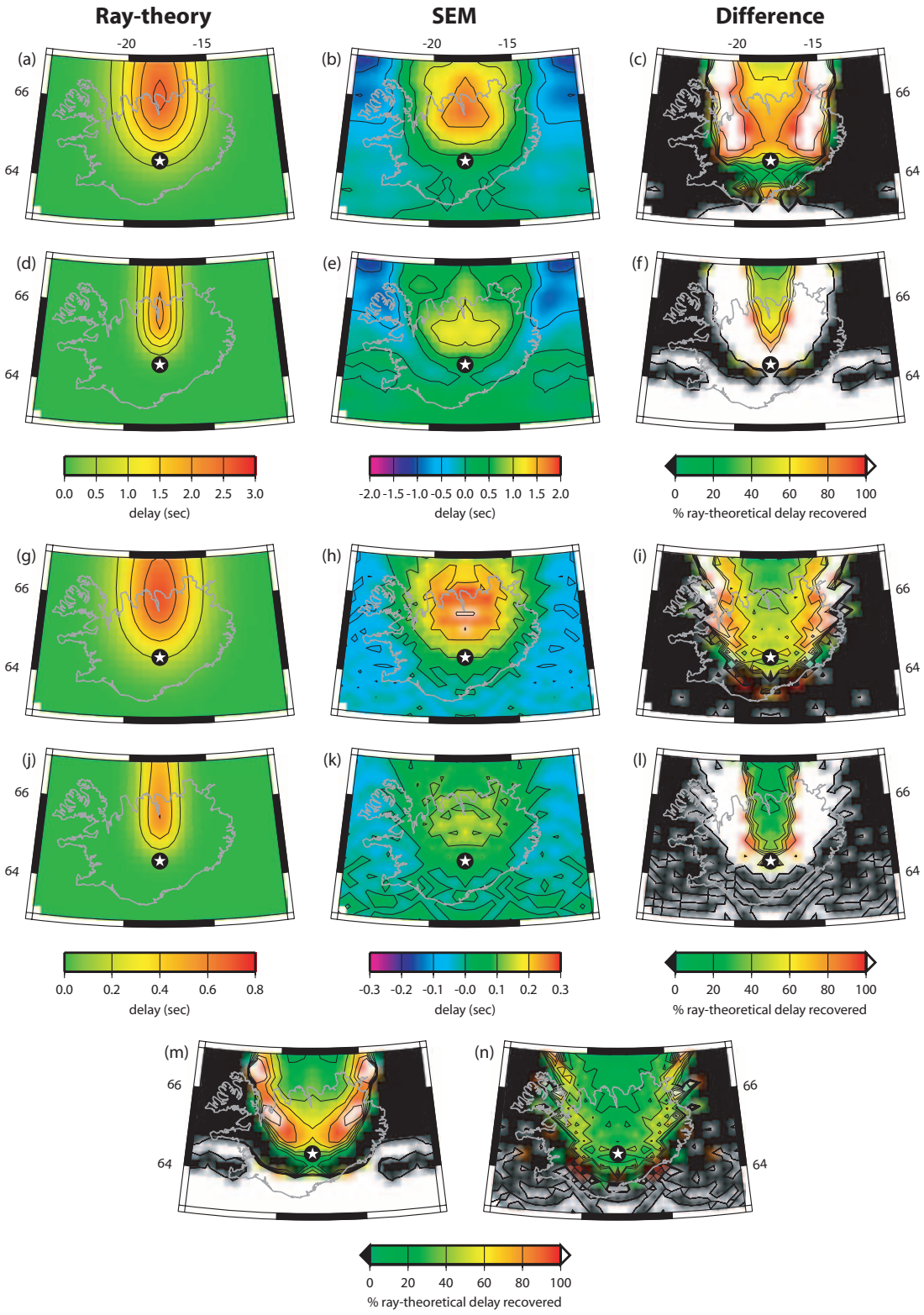

Figure 8. Comparison of ray-theoretical and SEM-synthetic traveltime delays for various low-velocity Gaussian-cross-sectional vertical cylinders (centre indicated by the star). Maps of ray-theoretical delay times, SEM-synthetic delay times and the percentage of the ray-theoretical delay recovered in the SEM-synthetic delay map are shown in the left, middle and right columns respectively for a hypothetical seismic source at 65° to the south. Maps (a)–(c) are for the *S*-wave arrival given a 100-km-radius, −4 per cent shear wave anomaly, maps (d)–(f) are also *S* delays but for a 50-km-radius, −6 per cent anomaly. Maps (g)–(l) are *P* delays and use 100-km-radius, −2 per cent anomaly (g)–(i), and a 50 km, −3 per cent anomaly (j)–(l). All four comparisons of SEM-synthetic delays with ray-theoretical delays show the broader delay footprint and smaller delay times of the SEM-synthetic delays. The percentage of the ray-theoretical delay from a 100-km-radius, −4 per cent shear-velocity anomaly recovered in an SEM-synthetic delay map calculated for a 50-km-radius, −6 per cent anomaly is shown in (m). The percentage of the ray-theoretical delay from a 100-km-radius, −2 per cent compressional-velocity anomaly recovered in an SEM-synthetic delay map calculated for a 50-km-radius, −3 per cent anomaly is shown in (n).

satisfactory results. The rms of the SEM-synthetic residuals is similar to that of the ray-theoretical residuals. Other SEM tests indicate that the upwelling conduit is probably a little narrower than in the ICEMAN models. This leads to the conclusion that the ICEMAN models are just one of a set of valid solutions. The satisfactory reproduction of traveltime delays using the ICEMAN models is perhaps a little surprising given the difference in the ray-theoretical and SEM-synthetic delay maps (Fig. 8). It is most likely a result of the smoothing imposed in the ray-theoretical inversion, which essentially broadens the sensitivity kernel of a traveltime observation. If the lengthscale of the imposed smoothing is similar to the width of the Fresnel zone, then a ray-theoretical inversion will result in a model from which the traveltime delays can be reproduced even when full wave propagation is accounted for. This explanation also leads to the conclusion that the ray-theoretical ICEMAN models represent end-members with the broadest, lowest velocity anomalies.

In a recent tomographic inversion of a similar teleseismic traveltime data set, finite-frequency sensitivity kernels were implemented (Hung *et al.* 2004). The Born–Fréchet kernel theory (a.k.a. banana-doughnut theory) used in this study accounts for the off-path 3-D sensitivity of seismic waves (Dahlen *et al.* 2000; Hung *et al.* 2000; Zhao *et al.* 2000) neglected by ray theory. In the finite-frequency inversion (Hung *et al.* 2004) the maximum depth of resolution is extended to the base of the upper mantle, rather than being limited to the upper ∼400 km as in ray-theoretical inversions (Wolfe *et al.* 1997; Foulger *et al.* 2001; Allen *et al.* 2002a). This is a result of the cross-sectional width of the sensitivity kernels, which stretches the sensitivities of the traveltime data set to greater depths. The same is true in the horizontal directions, the banana-doughnut kernels encompass a broader region than ray-theoretical sensitivities and the same data set therefore constrains a larger volume. While banana-doughnut kernels are a more accurate representation of traveltime sensitivities, inversions that utilize them are still subject to limitations in the resolution imposed by the data set, just as ray-theoretical inversions are. The philosophy behind the squeezing tests presented here is equally appropriate for finite-frequency inversions. For example, the depth-extent squeezing tests shown here (Fig. 3) are designed to determine if the low-velocity anomalies observed in the ICEMAN models at depth are the product of smearing along the ray path. Any such smearing is the product of limited data coverage and a minimum norm solution. The same squeezing tests could be used after a finite-frequency inversion to test the extent to which velocity anomalies are smeared within the 3-D sensitivity kernels.

Given the non-uniqueness of tomographic velocity models, there are two approaches to interpretation. Having conducted resolution experiments to determine a range of valid velocity structures, we either interpret only elements that are common to all the models, or we discuss the range of interpretations available. In the specific case of Iceland, all satisfactory velocity models show the presence of a low-velocity anomaly extending down to 350 km depth. The resolution and squeezing experiments shown here demonstrate that low velocities at greater depth could be the result of smearing along ray paths. The recent finite-frequency study of Iceland argues that low velocities do extend to the base of the upper mantle (Hung *et al.* 2004), which is consistent with several global tomographic models (e.g. Ritsema *et al.* 1999; Montelli *et al.* 2004). The horizontal extent of the low-velocity anomaly in the ICEMAN models represents an upper limit on its width. The ICEMAN-HP data set, which can be accurately modelled using ray theory, can be squeezed into a 100-km-wide cylinder. SEM experiments show that a 100-km-wide anomaly can generate a delay footprint twice as wide, indicating that a 100-km-wide anomaly could also satisfy the ICEMAN-LP and ICEMAN-S models. Tests with all three data sets demonstrate a trade-off between the anomaly width and amplitude: a narrower anomaly requires a higher peak velocity anomaly to maintain traveltime delays at the surface. However, differences in the ratio of velocity perturbation to anomaly width at higher and lower frequencies demonstrate that it is not possible to satisfy traveltime observations with a 100-km-wide velocity anomaly. This conclusion provides a lower bound on the width of the anomaly beneath Iceland. Given the resolution experiments presented above, we would conclude that the low-velocity anomaly beneath Iceland is between ∼75 and 100 km in radius (of the best-fitting Gaussian-shaped velocity anomaly).

The ICEMAN models also provide a lower bound on the amplitude of the velocity anomalies: −2 per cent for compressional waves and −4 per cent for shear waves. Geochemical constraints on the temperature anomaly beneath Iceland are in the range of 140–260 °C (McKenzie 1984; Schilling 1991; White *et al.* 1995; Shen *et al.* 2002). Using the temperature derivatives of Karato (1993) for olivine with a reasonable Q value, velocity anomalies of −2 and −4 per cent are easily interpreted in terms of temperature anomalies within the 140–260 °C range (Allen *et al.* 2002a). It is more difficult to put an upper limit on the amplitude of the velocity anomalies. Based on the results of the SEM experiments with a 50-km-radius plume, we estimated that peak velocity anomalies as high as −20 and −10 per cent for compressional and shear waves respectively would be required to maintain the traveltime delays at the surface. Although we have discounted an anomaly of this width and therefore velocity anomalies of this amplitude, we do expect the anomaly beneath Iceland to be narrower than the ICEMAN models. Correspondingly, the peak velocity anomalies would be expected to be greater than −2 and −4 per cent. Hung *et al.* (2004) account for wave front healing effects neglected by ray theory and estimate velocity anomalies that are 2–3 times greater than those in the ICEMAN models. The horizontal width of the anomaly Hung *et al.* (2004) resolve is also slightly greater than the ICEMAN models. Although they do not conduct squeezing tests, it is likely that they could also satisfy their data set with a narrower anomaly, which would require larger velocity anomalies still. Support for such large amplitude velocity anomalies is provided by a previous study of the diffraction effects of the Iceland anomaly, which concluded that the peak shear-velocity anomaly is −12 per cent (Allen *et al.* 1999).

We provide constraints on the range of velocity-anomaly geometries and amplitudes that may be present beneath Iceland. This range represents a constraint for geodynamic models of mantle processes beneath the Iceland hotspot. Top-down mechanisms for Iceland are driven by passive upflow into the new oceanic mantle, and lateral temperature gradients between the oceanic mantle and continental cratons. Geodynamic top-down models that aim to satisfy specific observations of the Iceland hotspot are not yet forthcoming. Perhaps one of the most difficult constraints to satisfy will be the requirement of a relatively narrow (<200 km diameter) cylindrical upwelling conduit at the centre of an oceanic mantle basin >1000 km wide (the width of the Atlantic ocean at the latitude of Iceland). Mantle plume, or bottom-up, models are available for the Iceland hotspot. The most recent models of Albers & Christensen (2001) and Ito (2001) prefer ultranarrow conduits 100 km in diameter. Our tests show that it is not possible to satisfy seismic observations with such a narrow conduit. Instead, the conduit must be >100 and <200 km in diameter. While our tests cannot provide tighter constraints on the range of conduit diameters, it is worth noting the implications of choosing a conduit at the narrower end of this range. Even with very low Q values of 100 for Q_P and 50 for Q_S, and a mantle temperature

at the upper limit of the geochemical range (260 °C), the maximum velocity anomalies resulting from temperature alone would be −3.6 and −6.0 per cent for compressional and shear waves, respectively (Karato 1993). Higher-amplitude velocity anomalies, as would be required by a conduit diameter closer to the 100-km end-member, would require the presence of partial melt or other fluids to greater than 350 km depth. The presence of high water concentrations in the mantle beneath Iceland (Nichols *et al.* 2002) would depress the solidus, increasing both the volume and depth of melting. While melting models for Iceland place most of the melting above 100 km depth, there is evidence for a small melt fraction at greater, as yet unconstrained, depths (Slater *et al.* 2001).

6 CONCLUSION

(i) While synthetic spike resolution tests give a sense of the extent and scale of resolution, they do not account for the limitations of the applied theory (usually ray theory) or the imposed effects of regularization (smoothing and damping). Squeezing experiments change the regularization and allow testing of alternative velocity-anomaly geometries (while satisfying the data to an equal extent) but still assume ray theory is valid. To test the significance of diffraction and wave front healing effects ignored by ray theory, and resulting in additional smoothing and damping of resolved velocity anomalies, respectively, full 3-D waveform propagation techniques must be applied.

(ii) When using teleseismic body wave arrival times measured at periods of around ∼20 s to constrain upper-mantle structure, finite-frequency effects are significant for velocity anomalies on the scale of ∼100 km or smaller, but significantly reduced for anomalies with lengthscales greater than ∼200 km. These lengthscales are similar to many mantle structures of interest, e.g. subducting slabs, backarc upwelling and mid-ocean ridge upwelling.

(iii) Our assessment of the true range of velocity anomalies beneath Iceland, based on testing using both ray-theoretical and finite-frequency techniques, shows the following.

(a) The ICEMAN velocity models are valid representations of Earth structure. This has been demonstrated through calculation of synthetic traveltimes using a numerical approach (SEM) that simulates seismic wave propagation through 3-D velocity models. The rms of the SEM-synthetic residuals is similar to the ray-theoretical residuals.

(b) The ICEMAN velocity models represent just one of a set of velocity models that satisfy the traveltime data set.

(c) The minimum depth extent of the low-velocity upwelling conduit beneath Iceland required by the regional ICEMAN data sets is ∼350 km.

(d) The upwelling conduit beneath Iceland is in the range of 100 to 200 km in horizontal diameter; it is most likely between 150 and 200 km.

(e) There is a trade-off between the horizontal diameter and amplitude of the peak-velocity anomaly. Given a 200 km diameter, the compressional- and shear-velocity anomalies are approximately −2 and −4 per cent, respectively. Given a narrower diameter, the amplitudes of the velocity anomalies increase. Perturbations greater than −10 per cent in both *P* and *S* velocity would be required for a 100-km-diameter upwelling.

(iv) Any top-down geodynamic model for the formation of Iceland must be capable of generating a low-velocity anomaly to greater than 350 km depth that is not more than 200 km in diameter. The model must produce such an upwelling at the centre of an ocean basin ∼1000 km wide.

(v) Bottom-up (or mantle plume) geodynamic models for Iceland must satisfy surface observations with a conduit greater than 100 km and less than 200 km in diameter. The lower bound of 100 km would also require a very large amplitude velocity anomaly that is difficult to justify without the presence of partial melt or other fluids to greater than 350 km depth. It is more likely that the true diameter is in the 150 to 200 km range. The minimum diameter bound also represents the required resolution of any future tomographic experiment designed to resolve the debate over the source depth of the upwelling, i.e. whether there is an upper- or lower-mantle origin for the Iceland hotspot.

ACKNOWLEDGMENTS

We thank Raul Madariaga, Jeroen Ritsema and an anonymous reviewer for helpful suggestions in preparing the manuscript. Support for RMA was provided by the Texaco Postdoctoral Fellowship awarded by the Seismological Laboratory of the California Institute of Technology and an award from the Graduate School of the University of Wisconsin–Madison, NSF-EAR 0309576 provided support for JT. The HOTSPOT and ICEMELT seismic data sets were provided by the IRIS-DMC and the SIL data set was provided by Vedurstofa Islands, Reykjavik, Iceland. Each figure has been generated using the GMT software of P. Wessel and W.H.F. Smith. This is contribution 9040 of the Division of Geological and Planetary Sciences, California Institute of Technology.

REFERENCES

Albers, M. & Christensen, U.R., 2001. Channeling of plume flow beneath mid-ocean ridges, *Earth planet. Sci. Lett.,* **187,** 207–220.

Allen, R.M. *et al.,* 1999. The thin hot plume beneath Iceland, *Geophys. J. Int.,* **137,** 51–63.

Allen, R.M. *et al.,* 2002a. Imaging the mantle beneath iceland using integrated seismological techniques, *J. geophys. Res.,* **107,** 2325, doi:10.1019/2001JB000595.

Allen, R.M. *et al.,* 2002b. Plume driven plumbing and crustal formation in iceland, *J. geophys. Res.,* **107,** 2163, doi:10.1029/2001JB000584.

Anderson, D.L., 1993. He-3 from the mantle — primordial signal or cosmic dust, *Science,* **261,** 170–176.

Anderson, D.L., 2001. A statistical test of the two reservoir model for helium isotopes, *Earth planet. Sci. Lett.,* **193,** 77–82.

Bijwaard, H. & Spakman, W., 1999. Tomographic evidence for a narrow whole mantle plume below Iceland, *Earth planet. Sci. Lett.,* **166,** 121–126.

Bjarnason, I.T., Wolfe, C.J. & Solomn, S.C., 1996. Initial results from the ICEMELT experiment: Body-wave delay times and shear-wave splitting across Iceland, *Geophys. Res. Lett.,* **23,** 459–462.

Breddam, K., Kurz, M.D. & Storey, M., 2000. Mapping out the conduit of the Iceland mantle plume with helium isotopes, *Earth planet. Sci. Lett.,* **176,** 45–55.

Dahlen, F.A., Hung, S.H. & Nolet, G., 2000. Frechet kernels for finite-frequency traveltimes—i. Theory, *Geophys. J. Int.,* **141,** 157–174.

Dziewonski, A.M. & Anderson, D.L., 1981. Preliminary reference earth model, *Phys. Earth planet. Int.,* **25,** 297–356.

Foulger, G.R. *et al.,* 2001. Seismic tomography shows that upwelling beneath iceland is confined to the upper mantle, *Geophys. J. Int.,* **146,** 504–530.

Graham, D.W., Castillo, P.R., Lupton, J.E. & Batiza, R., 1996. Correlated He and Sr isotope ratios in South Atlantic near- ridge seamounts and implications for mantle dynamics, *Earth planet. Sci. Lett.,* **144,** 491–503.

Hung, S.H., Dahlen, F.A. & Nolet, G., 2000. Frechet kernels for finite-frequency traveltimes—ii. Examples, *Geophys. J. Int.,* **141,** 175–203.

Hung, S.H., Dahlen, F.A. & Nolet, G., 2001. Wavefront healing: A banana-doughnut perspective, *Geophys. J. Int.,* **146,** 289–312.

Hung, S.H., Shen, Y. & Chiao, L.Y., 2004. Imaging seismic velocity structure beneath the Iceland hot spot: A finite frequency approach, *J. geophys. Res.,* **109,** B08305, doi:10.1029/2003JB002889.

Ito, G., 2001. Reykjanes 'V'-shaped ridges originating from a pulsing and dehydrating mantle plume, *Nature,* **411,** 681–684.

Ito, G., Lin, J. & Gable, C.W., 1996. Dynamics of mantle flow and melting at a ridge-centered hotspot; Iceland and the Mid-Atlantic ridge, *Earth planet. Sci. Lett.,* **144,** 53–74.

Ito, G., Shen, Y., Hirth, G. & Wolfe, C.J., 1999. Mantle flow, melting, and dehydration of the Iceland mantle plume, *Earth planet. Sci. Lett.,* **165,** 81–96.

Karato, S., 1993. Importance of anelasticity in the interpretation of seismic tomography, *Geophys. Res. Lett.,* **20,** 1623–1626.

King, S.D. & Anderson, D.L., 1998. Edge-driven convection, *Earth planet. Sci. Lett.,* **160,** 289–296.

Komatitsch, D. & Tromp, J., 2002a. Spectral-element simulations of global seismic wave propagation—I. Validation, *Geophys. J. Int.,* **149,** 390–412.

Komatitsch, D. & Tromp, J., 2002b. Spectral-element simulations of global seismic wave propagation—II. Three-dimensional models, oceans, rotation and self- gravitation, *Geophys. J. Int.,* **150,** 303–318.

Komatitsch, D., Ritsema, J. & Tromp, J., 2002. The spectral-element method, beowulf computing, and global seismology, *Science,* **298,** 1737–1742.

Korenaga, J. & Jordan, T.H., 2002. On the state of sublithospheric upper mantle beneath a supercontinent, *Geophys. J. Int.,* **149,** 179–189.

McKenzie, D., 1984. The generation and compaction of partially molten rock, *J. Petrol.,* **25,** 713–765.

Montelli, R., Nolet, G., Dahlen, F.A., Masters, G., Engdahl, E.R. & Hung, S.H., 2004. Finite-frequency tomography reveals a variety of plumes in the mantle, *Science,* **303,** 338–343.

Morgan, W.J., 1971. Convection plumes in the lower mantle, *Nature,* **230,** 42–43.

Nichols, A.R.L., Carroll, M.R. & Hoskuldsson, A., 2002. Is the Iceland hot spot also wet? Evidence from the water contents of undegassed submarine and subglacial pillow basalts, *Earth planet. Sci. Lett.,* **202,** 77–87.

Nolet, G. & Dahlen, F.A., 2000. Wave front healing and the evolution of seismic delay times, *J. geophys. Res.,* **105,** 19 043–19 054.

Ribe, N.M., Christensen, U.R. & Theissing, J., 1995. The dynamics of plume-ridge interaction. 1. Ridge-centered plumes, *Earth planet. Sci. Lett.,* **134,** 155–168.

Ritsema, J. & Allen, R.M., 2003. The elusive mantle plume, *Earth planet. Sci. Lett.,* **207,** 1–12.

Ritsema, J., van Heijst, H.J. & Woodhouse, J.H., 1999. Complex shear wave velocity structure imaged beneath Africa and Iceland, *Science,* **286,** 1925–1928.

Saltzer, R.L. & Humphreys, E.D., 1997. Upper mantle *P* wave velocity structure of the eastern snake river plain and its relationship to geodynamic models of the region, *J. geophys. Res.,* **102,** 11 829–11 841.

Schilling, J.G., 1991. Fluxes and excess temperatures of mantle plumes inferred from their interaction with migrating midocean ridges, *Nature,* **352,** 397–403.

Shen, Y. *et al.,* 2002. Seismic evidence for a tilted mante plume and north-south flow beneath Iceland, *Earth planet. Sci. Lett.,* **197,** 261–272.

Slater, L., McKenzie, D., Gronvold, K. & Shimizu, N., 2001. Melt generation and movement beneath Theistareykir, NE Iceland, *J. Petrol.,* **42,** 321–354.

Stefansson, R. *et al.,* 1993. Earthquake prediction research in the south Iceland seismic zone and the SIL project, *Bull. seism. Soc. Am.,* **83,** 696–716.

Wielandt, E., 1987. On the validity of the ray approximation for interpreting delay times, in *Seismictomography; with applications in global seismology and exploration geophysics*, pp. 85–98, ed. Nolet, G., D. Reidel Publishing Company, Dordrecht, Netherlands.

White, R.S., Bown, J.W. & Smallwood, J.R., 1995. The temperature of the iceland plume and origin of outward- propagating v-shaped ridges, *J. Geol. Soc.,* **152,** 1039–1045.

Wolfe, C.-J., Bjarnason, I.-T., VanDecar, J.-C. & Solomon, S.-C., 1997. Seismic structure of the Iceland mantle plume, *Nature,* **385,** 245–247.

Zhao, D., 2001. Seismic structure and origin of hotspots and mantle plumes, *Earth planet. Sci. Lett.,* **192,** 251–265.

Zhao, L., Jordan, T.H. & Chapman, C.H., 2000. Three-dimensional frechet differential kernels for seismic delay times, *Geophys. J. Int.,* **141,** 558–576.